

SRCN3D: Sparse R-CNN 3D Surround-View Camera Object Detection and Tracking for Autonomous Driving

Yining Shi, Jingyan Shen, Yifan Sun, Yunlong Wang, Jiaxin Li, Shiqi Sun, Kun Jiang*, Diange Yang*
Tsinghua University

Abstract

Detection and tracking of moving objects (DATMO) is an essential component in environmental perception for autonomous driving. In the flourishing field of multi-view 3D camera-based detectors, different transformer-based pipelines are designed to learn queries in 3D space from 2D feature maps of perspective views, but the dominant dense cross-attention mechanism between queries to values is computationally inefficient. This paper proposes Sparse R-CNN 3D (SRCN3D), a novel two-stage fully-sparse detector with sparse queries, sparse attention and sparse prediction for surround-view camera detection and tracking. SRCN3D adopts a cascade structure with twin-track update of both fixed number of proposal boxes and latent proposal features. Compared to prior arts, our novel sparse feature sampling module only utilizes local 2D region of interest (RoI) features calculated by projection of 3D proposal boxes for further box refinement, leading to an effective, fast and lightweight pipeline. For multi-object tracking, motion features, proposal features and RoI features are comprehensively utilized in multi-hypotheses data association. Extensive experiments on nuScenes dataset demonstrate that SRCN3D achieves competitive performance in object detection and surpasses previous best arts before 2022.08.09 in camera-only multi-object tracking by more than 10 points in terms of AMOTA metric.

Introduction

Environmental perception is an essential task in autonomous driving. 3D object detection and tracking is responsible for classifying and localizing objects of interest, as well as recording their unique labels and past trajectories. Compared to LiDAR, on-board cameras have the advantages of lower cost, wider detection range, higher angular resolution, and richer semantic cues. However, there are two long-standing challenges existing for vision-centric detectors. As cameras have no geometric or depth cues, 3D reconstruction is an ill-conditioned problem. Another issue is cross-view fusion, namely, where two adjacent cameras see parts of one object, but need to detect it as a whole.

Vision-centric detectors rise rapidly in accuracy thanks to latest innovation of data-driven view transformation from perspective view to 3D world space. LSS (Phillion and Fidler 2020) puts forward an geometry based explicit pipeline consisting of depth estimation, pointcloud lifting, voxelization and splatting, while DETR3D(Wang et al. 2021b) brings up

a network based implicit pipeline learning queries from projected reference points to get values without explicit depth estimation and post-processing. As shown in Fig. 1, previous arts require either dense queries or dense interaction between queries and values. Our proposed method enjoys the merit of implicit pipeline and avoids dense feature sampling at the same time.

Our proposed method, SRCN3D is a simple cascade pipeline and set prediction approach highly inspired by Sparse R-CNN (Sun et al. 2021). We adopt commonly used backbones and Feature Pyramid Network (FPN) (Lin et al. 2017a) neck, but a novel SRCN3D head which iteratively updates both 3D proposal boxes and proposal features at the same time. Proposal boxes are projected to six views to aggregate local RoI features. Based on that, proposal features are refined via a dynamic instance interactive (DII) head, which then generates classification and the offsets applied to original bounding boxes. After six stages, the final refined proposal boxes are directly detection outputs without the need of complicated post-processing step or regression process from latent features. Our framework is free of transformer-style operations such as masking operation or positional embeddings.

Furthermore, in a mainstream tracking-by-detection (TBD) pipeline, multi-object tracking is challenging in data association process given possible missed or false detection. This problem is more common for camera-based detectors than LiDAR-based detectors. Therefore, conventional deterministic data association suffers from poor track continuity. Recent trackers, such as QD-3DT (Hu et al. 2022), incorporate dense image features, while re-identification (Re-ID) from dense region proposals is inefficient and inaccurate. In light of instability of detection results, we find that a simplified multi-hypotheses Random Finite Set (RFS) approach for probabilistic matching reduces failed tracking. Our proposed tracker is also the first approach to incorporate RoI features and proposal features in RFS framework.

In summary, the contributions of this paper can be summed up as follows:

- To the best of our knowledge, **the first two-stage network-based 3D→2D multi-view camera 3D object detection approach without transformer-style component**. The pipeline is straightforward, lightweight, and faster than transformer-based detectors.

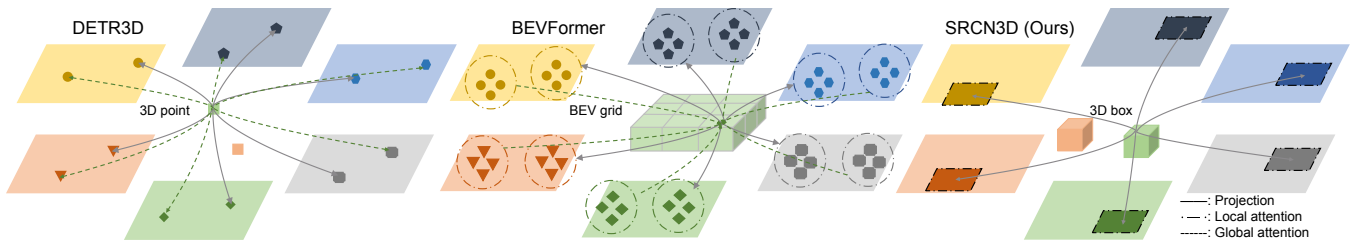


Figure 1: Comparison between typical Multi-View 3D (MV3D) detectors. DETR3D (Wang et al. 2021b) applies sparse queries and dense global attention. BEVFormer (Li et al. 2022) applies dense queries and dense deformable attention. SRCN3D steps further to sparser queries and totally sparse local RoI attention, which pioneers a fully-sparse paradigm.

- **A novel sparse cross-attention module to refine 3D proposals from 2D feature maps**, which replaces dense attention with local sparse dynamic instance interaction module and involves fewer queries. Consequently, lower computation cost is achieved.
- **A novel probabilistic feature-embedding multi-object tracking approach**, which takes advantage of hybrid motion features, proposal features and RoI features in data association process, and achieves state-of-the-art performance.

Related Work

Multi-camera 3D Object Detection

MV3D is recently considered plausible thanks to data-driven view transformation and rapidly increasing performance. There are three paradigms of state-of-the-art multi-view camera 3D object detectors, which are $2D+BEV$, $2D \rightarrow 3D$, and $3D \rightarrow 2D$. $2D+BEV$ is to predict 3D boxes from perspective view 2D images and perform BEV aggregation (Wang et al. 2021a, 2022; Zhang et al. 2022a; Park et al. 2021), having difficulty in cross-view fusion. $2D \rightarrow 3D$ performs depth estimation, then transforms to world coordinate and aggregates pointclouds (Huang et al. 2021; Huang and Huang 2022) in a bottom-up fashion, but is sensitive to depth errors. $3D \rightarrow 2D$ proposes 3D queries randomly, then undergoes a cascade refinement (Wang et al. 2021b; Liu et al. 2022a; Li et al. 2022), without depth estimation. Our proposed method adopts the $3D \rightarrow 2D$ paradigm and designs a novel two-stage pipeline which is different from previous single-stage arts.

Transformer-based Object Detection

Vision transformers have demonstrated excellent performance in object detection. In 2D domain, DETR (Carion et al. 2020) presents a set-prediction paradigm with regard to a fixed set of objects. Deformable DETR (Zhu et al. 2020) invents deformable attention for faster convergence. Furthermore, Sparse R-CNN (Sun et al. 2021) puts forward a completely sparse schema, where each proposal box interacts only with its specific proposal feature. In 3D domain, transformers serve as cross-attention between 3D queries and 2D feature maps (Wang et al. 2021b; Li et al. 2022; Liu et al. 2022a,b). DETR3D (Wang et al. 2021b) is the first to apply a top-down framework, which projects reference points on feature maps

and performs cross-attention to refine proposal features. BEVFormer (Li et al. 2022) leverages cross-attention on bird’s eye view (BEV) grid features, and employs spatial deformable attention for BEV grids and temporal alignment of BEV features. PETR (Liu et al. 2022a) and PETRv2 (Liu et al. 2022b) adopt idea from implicit neural representation and project 2D features map to 3D space so as to interact with 3D queries. Compared to dense attention arts, our method explores a sparse feature sampling module without global attention and makes itself a purely sparse approach.

3D Multi-Object Tracking

MOT is another challenging task right after object detection, aiming to temporally associate trajectories of each same object and record its unique label. Data association is the core issue of MOT, where the dominant matching approach is Global Nearest Neighbor (GNN), carried out in the form of Hungarian or Greedy algorithm used in AB3DMOT (Weng et al. 2020). Another approach is RFS (García-Fernández et al. 2017), an online multi-hypotheses paradigm circumventing deterministic one-to-one pair matching. Current MOT researches, e.g. CenterTrack (Zhou, Koltun, and Krähenbühl 2020), QD-3DT (Hu et al. 2022) and MUTR3D (Zhang et al. 2022b), focus on utilizing implicit features to express matching similarity in the embedded space, empowering the network to identify the same object based on appearance features through re-identification (Re-ID) process. Our tracker explores a novel multi-hypotheses probabilistic mode of data association with hybrid feature embedding.

Sparse R-CNN 3D

Overview

The overall framework of SRCN3D is illustrated in Fig. 2. SRCN3D has a novel two-stage fully-convolutional 3D object detection architecture.

The architecture of SRCN3D consists of a common backbone with FPN and a novel SRCN3D head. First of all, we feed the RGB images into a backbone network (e.g. ResNet-101 (He et al. 2016)) with FPN (Lin et al. 2017a) to generate multi-level multi-camera feature maps $\{F_1^i, F_2^i, F_3^i, F_4^i\}_{i=1}^{N_{cam}}$ for each view. As the beginning of SRCN3D head, we start from a fixed set of 3D learnable proposal boxes and proposal features, and the initial parameters for boxes and features are randomly initialized and learnable during training process. In

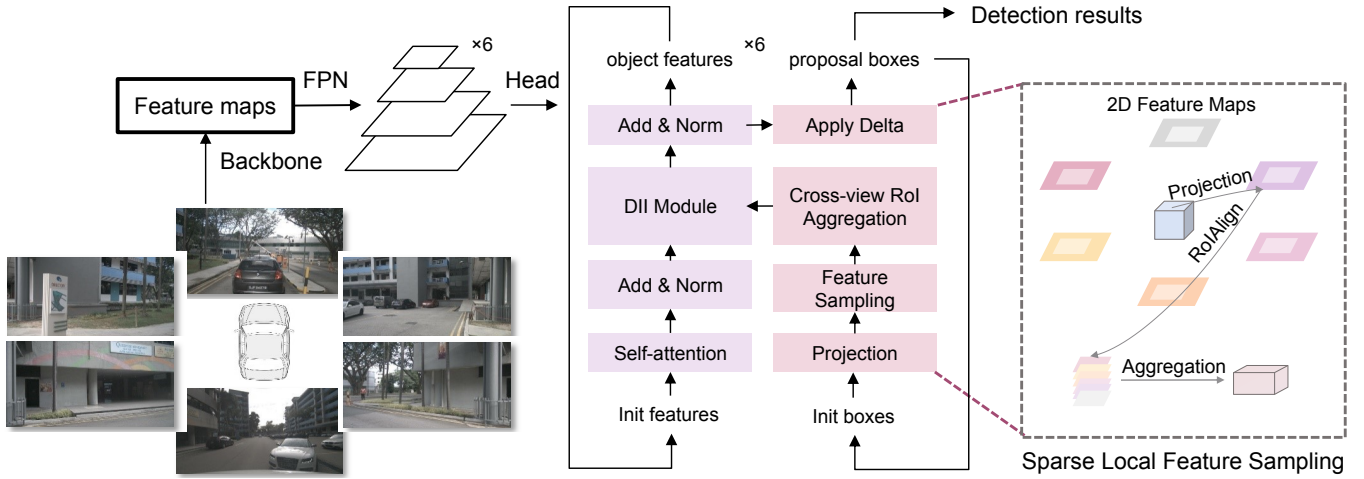


Figure 2: The framework of SRCN3D. Taken camera images as inputs, SRCN3D contains a backbone network with FPN to extract 2D feature maps and a twin-track detection module. A sparse feature sampling module is designed to extract local ROI features and refine the proposal boxes.

a cascade structure, the proposal boxes and proposal features compose strict pairs while non-pairs do not interact. Boxes and features are updated in a twin-track approach. Proposal boxes are updated in a box adjustment step and proposal features are updated with a sparse feature sampling module. Last stage of proposal boxes and class regression of proposal features without post-processing techniques comprise the final results.

SRCN3D Head

As shown in Fig. 3, SRCN3D head composes of three key modules, that is, a sparse feature sampling module for feature extraction, a 3D DII module for feature refinement and a box adjustment module for box refinement. For each round of iteration there are two inputs, namely a fixed number of learnable proposal boxes and proposal features. Each round of bounding box forward process includes the following steps:

- Restore proposal boxes to world scale, get eight corner points and project corner points to images using different intrinsic and extrinsic camera parameters.
- Collect four borderline corner points on each images to form a ROI candidate, sample ROI features using RoIAlign and aggregate cross-view ROI features as input of DII head.
- Undergo 3D DII head for refinement of object features and output cues (fine-tuning values) for box adjustment.
- Refine location, dimension, rotation and velocity with box adjustment module, operate normalization on 3D position of boxes and prepare the input for the next round.

DII head is a light convolutional design and shows great performance with lower computation cost in 2D object detection (Sun et al. 2021). There is a multi-head attention module between features, and then two 1×1 convolutional layers are designed in DII head for interaction, followed by a Feed-Forward Network (FFN) block with layer normalization and a linear projection block to output classification and regression

predictions. Local interaction is implemented by applying 1×1 convolutional kernels on ROI features extracted from proposal boxes and generating corresponding parameters based on proposal features through linear transformation.

3D proposal boxes are defined as a fixed number of boxes parameterized to the same dimension as 3D bounding box (e.g. $\{B_i\}_{i=1}^N \subset R^{10}, N = 300$). The 10 dimensions are defined as $[c_x, c_y, h, w, c_z, l, \cos\theta, \sin\theta, v_x, v_y]$, where c_x, c_y, c_z are center coordinates of the box, h, w, l are height, weight and length, θ is the yaw angle and v_x, v_y are velocities.

Proposal features are represented by sets of high-dimensional latent vectors (e.g. $\{f_i\}_{i=1}^N \subset R^{256}$), strictly corresponding to 3D proposal boxes.

Sparse Feature Sampling Module. Learnable 3D boxes are sparse candidates updated iteratively. We decode 3D proposal boxes from center points to box corners through simple geometric transformation. For simplicity, we refer i th decoded box $\{C_{il}\}_{l=1}^8 \subset R^3$ with coordinates of eight corners. Through a standard camera model, these proposal boxes are projected into visible regions of cameras as follows:

$$C_{il}^* = C_{il} \oplus 1, C_{mil} = T_m C_{il}^*, \quad (1)$$

where $l = 1, \dots, 8, m = 1, \dots, N_{cam}, C_{mil} = (c_{milx}, c_{mily}, 1)$ and T_m denotes the camera transformation matrix. Then the projected boxes on each camera can be obtained as follows:

$$\tilde{B}_{im} = (\min_l c_{mlx}, \min_l c_{mly}, \max_l c_{mlx}, \max_l c_{mly}), \quad (2)$$

where $i = 1, \dots, N, m = 1, \dots, N_{cam}$.

As shown in Fig. 3, given the projected boxes, we use RoIAlign operation to extract features of interest. The projection of box corner points may result in three cases. The normal case indicates a projected 2D box on images. If the projected points have a negative depth, the box locates behind the camera, which is naturally invisible. If the projected corners are outside or partially outside the pixel space, the

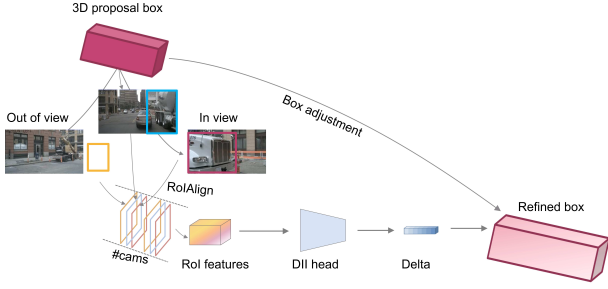


Figure 3: A graphical illustration of sparse feature sampling module. 3D proposal boxes are initialized and projected into feature maps in the camera plane for ROI extraction. After aggregation, ROI features interact with proposal features in DII head which produces cues for refinement. Finally, box adjustment module refines the boxes.

box is (partially) invisible. The latter two abnormal feature sampling cases result in empty or partially empty ROI features via RoIAlign, so that masking operations and positional encoding techniques are deftly avoided.

Cross-view fusion. Before entering the prediction head, corresponding ROI features on multi-view camera images are aggregated to guarantee cross-view fusion learning. In this way, ROI features maintain a fixed expression, no matter how many cameras capture one proposal box.

Box Adjustment

Here we define the predicted boxes and cues in t th stage as $\{b_i^t\}_{i=1}^N$ and $\{\Delta b_i^t\}_{i=1}^N$ respectively. Then the box adjustment operation for location and dimension parameters can be formulated as follows:

$$\begin{cases} b_{ix}^{t+1} = \Delta b_{ix}^{t+1} \times b_{iw}^t + b_{ix}^t \\ b_{iy}^{t+1} = \Delta b_{iy}^{t+1} \times b_{il}^t + b_{iy}^t \\ b_{iz}^{t+1} = \Delta b_{iz}^{t+1} \times b_{ih}^t + b_{iz}^t \end{cases} \quad (3)$$

Considering non-negative constraints, dimension parameters are usually in the form of logarithm. Therefore, its adjustment is formulated as follows:

$$\begin{cases} b_{iw}^{t+1} = e^{\Delta b_{iw}^{t+1}} \times b_{iw}^t \\ b_{il}^{t+1} = e^{\Delta b_{il}^{t+1}} \times b_{il}^t \\ b_{ih}^{t+1} = e^{\Delta b_{ih}^{t+1}} \times b_{ih}^t \end{cases} \quad (4)$$

As for rotation and velocity, we directly take the values in $\{\Delta b_i^t\}_{i=1}^N$ as the predicted results of t th stage.

Loss Design

Generally, the loss function of SRCN3D is a linear combination of a Focal Loss (Lin et al. 2017b) for category classification and a L1 norm loss for 3D bounding box regression, which is as follows:

$$\mathcal{L} = \omega_{cls} \times \mathcal{L}_{cls} + \omega_{reg} \times \mathcal{L}_1. \quad (5)$$

SRCN3D employs set prediction loss following DETR (Carion et al. 2020). Details of set prediction loss are presented in the supplementary material.

Multi-object Tracking

Multi-object Tracking mainly handles data association of detected objects between past and current frames. Given unsatisfactory detection results, we adopt a hypothesis-oriented probabilistic approach, Multi-Bernoulli Mixture (MBM) to deal with uncertain data association. MBM treats data association into global hypotheses and single target hypotheses. The MBM density is defined as sum of j global hypotheses as follows:

$$f^{\text{mbm}}(X) \propto \sum_j \sum_{X_1 \cup \dots \cup X_n = X} \prod_{i=1}^n w_{j,i} f_{j,i}(X_i), \quad (6)$$

where $f^{\text{mbm}}(X)$ is the posterior of MBM intensity, X is the whole set of detected objects, $w_{j,i}$ indicates the weight of a Bernoulli component X_i in global hypothesis j , and $f_{j,i}(X_i)$ is the probability intensity of single Bernoulli component X_i in global hypothesis j , defined as follows:

$$f_{j,i}(X_i) = \begin{cases} 1 - r_{j,i} & \text{if } X_i = \emptyset \\ r_{j,i} p_{j,i}(x) & \text{if } X_i = x \\ 0 & \text{otherwise} \end{cases}, \quad (7)$$

where $r_{j,i}$ denotes the existence probability of object x in single target hypothesis (STH) X and $p_{j,i}$ is the probability density function considering the log likelihood of the hypothesis target. Each STH denotes one object detected or a missed detection. Temporal prediction and update of states follow a standard unscented kalman filter (UKF). Important criterion for matching is to compute likelihood between measurements and states. In SRCN3D tracker, each measurement includes explicit properties of 3D bounding boxes and two kinds of implicit features, namely, ROI features and proposal features. The likelihood of 3D bounding boxes is computed by Mahalanobis distance introduced in (Chiu et al. 2021), and latent ROI features and proposal features follow a cosine similarity. The overall likelihood is calculated as

$$l = l_{box} + \alpha \times l_{RoI} + \beta \times l_{prop}. \quad (8)$$

In practice, we set $\alpha = \beta = 0.5$ to achieve an balance among box attributes and appearance.

Experiments

Dataset

We report experiment results on large-scale public nuScenes dataset (Caesar et al. 2020), which includes 1000 driving scenes of about 20 seconds duration. RGB images are collected from 6 cameras with known intrinsic and extrinsic camera parameters. NuScenes dataset provides 28130, 6019 and 6008 samples for training, validation and testing, respectively. Only key frames at 2Hz are annotated and used.

Metrics

We adopt the nuScenes (Caesar et al. 2020) official evaluation protocol. As for detection metrics, we adopt mean average precision (mAP) and nuScenes Detection Score (NDS) as primary metrics, and true positive metrics (TP metrics) including average translation error (ATE), average scale error

Method	Size	Backbone	NDS \uparrow	mAP \uparrow	mATE \downarrow	mASE \downarrow	mAOE \downarrow	mAVE \downarrow	mAAE \downarrow
CenterNet (Duan et al. 2019)	-	DLA	0.328	0.306	0.716	0.264	0.609	1.426	0.658
FCOS3D ‡#(Wang et al. 2021a)	1600 \times 900	Res-101	0.415	0.343	0.725	0.263	0.422	1.292	0.153
DETR3D ¶(Wang et al. 2021b)	1600 \times 900	Res-101	0.425	0.346	0.773	0.268	0.383	0.842	0.216
BEVDet §(Huang et al. 2021)	1056 \times 384	Res-101	0.396	0.330	0.702	0.272	0.534	0.932	0.251
BEVFormer-S ¶(Li et al. 2022)	1600 \times 900	Res-101	0.448	0.375	0.725	0.272	0.391	0.802	0.200
PETR §¶(Liu et al. 2022a)	1600 \times 900	Res-101	0.442	0.370	0.711	0.267	0.383	0.865	0.201
SRCN3D (Ours)¶	1600 \times 900	Res-101	0.428	0.337	0.779	0.287	0.367	0.781	0.188
SRCN3D (Ours)¶	1600 \times 900	V2-99	0.475	0.396	0.737	0.294	0.278	0.728	0.197

Table 1: Comparison of state-of-the-art detectors on nuScenes detection val set. ‡: with test-time augmentation. §: trained with CBGS (Zhu et al. 2019). ¶: initialized from pretrained FCOS3D (Wang et al. 2021a) backbone. #: with model ensemble.

Method	NDS \uparrow	mAP \uparrow	mATE \downarrow	mASE \downarrow	mAOE \downarrow	mAVE \downarrow	mAAE \downarrow
CenterNet (Duan et al. 2019)	0.400	0.338	0.658	0.255	0.629	1.629	0.142
EPro-PnP-Det(Chen et al. 2022a)	0.453	0.373	0.605	0.243	0.359	1.067	0.124
M2BEV(Xie et al. 2022)	0.451	0.398	0.577	0.245	0.500	1.227	0.154
FCOS3D ‡(Wang et al. 2021a)	0.428	0.358	0.690	0.249	0.452	1.434	0.124
BEVFormer-S (Li et al. 2022)	0.462	0.409	0.650	0.261	0.439	0.925	0.147
DETR3D †(Wang et al. 2021b)	0.479	0.412	0.641	0.255	0.394	0.845	0.133
DD3D †‡(Park et al. 2021)	0.477	0.418	0.572	0.249	0.368	1.014	0.124
BEVDet †(Huang et al. 2021)	0.488	0.424	0.524	0.242	0.373	0.950	0.148
PETR †(Liu et al. 2022a)	0.504	0.441	0.593	0.249	0.383	0.808	0.132
SRCN3D †(Ours)	0.463	0.396	0.673	0.269	0.403	0.875	0.129

Table 2: Comparison of state-of-the-art detectors on nuScenes detection test set. Detection methods using temporal aggregation are not included. †: trained using extra data. ‡: with test time augmentation.

(ASE), average orientation error (AOE), average velocity error (AVE), and average attribute error (AAE). Metrics of MOT are based on CLEARMOT (Bernardin and Stiefelhagen 2008), including average multi object tracking accuracy (AMOTA) as the primary metric, and average multi object tracking precision (AMOTP) and recall rate (RECALL). Reports of SRCN3D on all detection and tracking metrics are publicly available on nuScenes leaderboard.

Training and Inference

Training. Our code is built upon the MMDetection3D (MMDetection3D Contributors 2020) infrastructure. We employ two types of backbone network: (1) ResNet101 (He et al. 2016) pretrained on FCOS3D (Wang et al. 2021a) and PGD (Wang et al. 2022), (2) VoVNetV2-99 (Lee and Park 2020) pretrained on DD3D (Park et al. 2021). We use a bipartite loss via 3D Hungarian assigner, which consists of a Focal Loss (Lin et al. 2017b) with weight 2.0 and a L1 loss with weight 0.25. The model is trained using AdamW optimizer with weight decay of 0.01. The learning rate is initialized with $2e^{-4}$ and decays with cosine annealing policy. We set the detection region to $[-61.2m, 61.2m]$ for the X and Y axis, and $[-5m, 3m]$ for the Z axis. Experiments are trained for 24 epochs on 8 2080TI GPUs, the training hours is around 24 hours.

Inference. In the inference process, SRCN3D makes simple predictions without any post-processing step such as NMS and test-time augmentation (TTA).

Comparison with state-of-the-art

nuScenes detection benchmark. In Table. 1, we present the performance comparison with state-of-the-art methods on nuScenes validation set. SRCN3D gains 42.8% NDS and 33.8% mAP for ResNet101 (He et al. 2016) backbone and image size of 900×1600 . Compared to Monocular 3D detectors, SRCN3D surpasses CenterNet (Duan et al. 2019) and FCOS3D (Wang et al. 2021a) in NDS by 10.1% and 1.3%. Compared to MV3D detectors, SRCN3D also shows competitive results. Under the same backbone and image size settings, our method outperforms DETR3D (Wang et al. 2021b) by 0.3% in NDS. Moreover, our model infers within 2.9 FPS on a single RTX3090 GPU, faster than dense transformer-based detectors like DETR3D (Wang et al. 2021b) (2.7 FPS) and BEVFormer (Li et al. 2022) (2.1 FPS). In terms of TP metrics, it shows that SRCN3D works well in predicting orientation, velocity and attributes, achieving the best performance in mAOE and mAVE. However, SRCN3D still suffer from limitations for translation and scale predictions, which could be further improved. Table. 2 shows the performance comparison on nuScenes detection test set. Our method achieves competitive performance on NDS, mAP and other true positive metrics. Overall, the experimental results demonstrate the effectiveness of our method on 3D object detection task.

nuScenes tracking benchmark. Table. 3 reports nuScenes tracking benchmark on both validation and test split. SRCN3D achieves state-of-the-art performance in camera track and exceeds other competitors by a large margin. On validation set, compared with camera based methods,

Method	Modality	Split	AMOTA \uparrow	AMOTP \downarrow	RECALL \uparrow
QD3DT(Hu et al. 2022)	C	val	0.242	1.518	0.399
MUTR3D(Zhang et al. 2022b)	C	val	0.294	1.498	0.427
ViP3D(Gu et al. 2022)	C	val	0.216	1.616	0.358
SRCN3D (Ours)	C	val	0.439	1.280	0.545
CenterTrack-Open (Zhou, Koltun, and Krähenbühl 2020)	L + C	test	0.108	0.989	0.412
QD-3DT (Hu et al. 2022)	C	test	0.217	1.550	0.375
PolarDETR (Chen et al. 2022b)	C	test	0.273	1.185	0.404
DEFT (Chaabane et al. 2021)	C	test	0.177	1.564	0.338
MUTR3D(Zhang et al. 2022b)	C	test	0.270	1.494	0.411
SRCN3D (Ours)	C	test	0.398	1.317	0.538

Table 3: Comparison of state-of-the-art trackers on nuScenes tracking benchmark. Quantitative results of val set are from original paper and test set from nuScenes leaderboard. For modalities, “L” denotes LiDAR and “C” denotes camera.

SRCN3D achieves the best performance in all reported metrics. On test set, our method ranks top on nuScenes tracking leaderboard (2022.8.9), which achieves 0.398 in terms of AMOTA metrics on nuScenes test set, more than 12 points of accuracy improvement over recent state-of-the-art camera-only trackers. The test results also show a moderate AMOTP error and the highest recall rate.

Ablation Study

In this section, we perform ablations on several important components or properties of SRCN3D on nuScenes validation set.

Box	DII	Delta	Init	NDS \uparrow	mAP \uparrow
✓			Random	0.310	0.249
	✓		Random	0.341	0.258
✓	✓		Random	0.409	0.333
✓	✓	✓	Fixed	0.414	0.329
✓	✓	✓	Random	0.428	0.337

Table 4: Ablation on key modules. “Box” denotes two-stage proposal boxes module. “DII” denotes dynamic instance interaction head. “Delta” denotes the box adjustment module. “Init” denotes initialization method for proposal boxes.

Backbone	Proposals	Objects	Stages	NDS \uparrow	mAP \uparrow
R-101	900	300	6	0.428	0.337
R-101	500	300	6	0.408	0.332
R-101	300	300	6	0.418	0.327
V2-99	900	300	6	0.475	0.396
V2-99	500	300	6	0.474	0.378
R-101	300	300	6	0.418	0.327
R-101	300	200	6	0.410	0.324
R-101	900	300	6	0.428	0.337
R-101	900	300	3	0.421	0.335
R-101	900	300	1	0.385	0.297

Table 5: Ablation on the number of proposals, candidate objects and stages.

Modules	AMOTA \uparrow	AMOTP \downarrow	RECALL \uparrow
DE	0.277	1.519	0.506
PR	0.405	1.361	0.508
PR + R	0.436	1.287	0.539
PR + H	0.439	1.280	0.545

Table 6: Ablation of the tracking module. Deterministic method is our adaption of AB3DMOT (Weng et al. 2020). The other lines shows utilization of different features in data association process. “DE” denotes deterministic matching method. “PR” denotes probabilistic matching method. “R”, and “H” denotes RoI features and hybrid features, respectively.

Ablation on key modules. We point out four key modules for SRCN3D completely different from previous arts, which are learnable boxes, DII module, box adjustment and initialization. Ablation is implemented by replacing these modules in SRCN3D with similar parts in DETR3D (Wang et al. 2021b). Table. 4 shows impacts of the four key modules. The first case constructs a two-stage DETR3D, showing that query features are not sufficient to refine proposal boxes. Model without DII head uses global attention weights to get global attention between proposals and apply average pooling of RoI features. The second case is where boxes are regressed directly by a regression branch of proposal features at the beginning. The third case, without box adjustment step, produces boxes estimation by directly inputting object features after DII head into regression branch, showing slightly reduced accuracy. Moreover, random initialization of proposal boxes reports better results than fixed counterparts. Ablation demonstrates that our key modules are indispensable in the framework.

Ablation on number of proposals, objects and stages. The number of proposal box and feature is related to GPU memory cost and inference speed. Number of objects determines the output of NMS-free box coder. Number of stages refers to how many times the proposal boxes are refined.

Table. 5 indicates that the quantitative results only show slight decrease ($< 3\%$) when reducing number of proposals to lower amounts. On the other hand, decreasing candidate

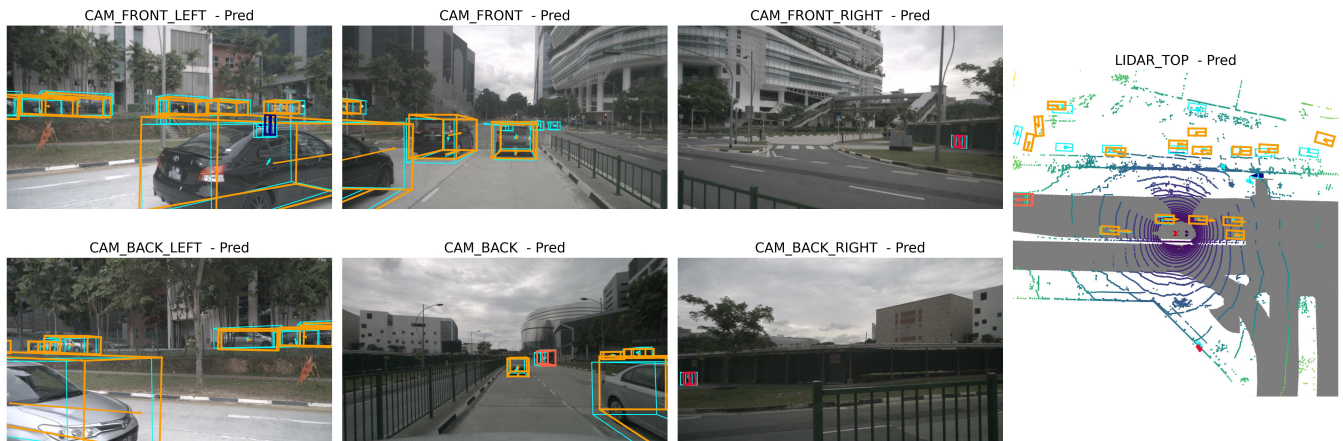


Figure 4: Visualization of final predictions and ground truth boxes on nuScenes val set. Ground truth boxes are coloured in light green. Boxes coloured in orange, red and blue correspond to vehicles, bicycles and pedestrians, respectively.

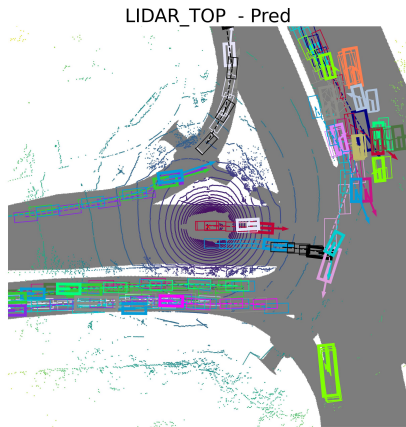


Figure 5: Visualization of tracking results on nuScenes val set. We visualize the tracked objects in the past five key frames in the same scene. Boxes in different colors refer to different tracked instances.

objects of final detection may hurt more accuracy. Moreover, for stages in cascade structure, as output of each stage is considered in later loss computation, the first three stages play a more significant role in improving accuracy, while from stage three to six the box refinement process is nearly saturated. Ablation of these three properties demonstrates that our sparse feature sampling module is capable to capture region of interests with only local features in a lightweight manner.

Ablation on tracking module. As shown in Table. 6, for camera-only tracking, probabilistic association greatly outperforms deterministic counterparts. We further demonstrate that as RoI features and proposal features represent kinds of affinity cues for appearance and classification respectively, these latent features facilitate the matching process and improve tracking precision.

Visualization

Fig. 4 visualizes final detection results in the camera front view and bird’s-eye view on the validation set with ground truth annotation. Overall, as shown in the bird’s-eye view, the predicted boxes are close to the ground truth ones. The bus detected as a whole both in front and left-front camera illustrates the effectiveness of cross-view fusion in overlapped regions. Small objects (e.g. pedestrians in the front-left camera view) are also detected precisely. These results indicate a satisfactory performance of SRCN3D and related modules. More visualizations of final results and intermediate-stage proposal boxes are available in the supplementary materials.

Fig. 5 present a BEV example of tracking on nuScenes validation set. We visualize past five key frames of unique objects in a crowded intersection to demonstrate satisfactory tracking accuracy and continuity.

Visualization also exposes current limitations of SRCN3D. In areas where features of targeted objects are dense, the predicted boxes overlap with each other, which is unreasonable for real-world objects. It shows that there remains a few duplicates in predicted boxes.

Conclusion

This paper proposes a novel innovative architecture, SRCN3D, aiming at detecting and tracking objects of interest. It possesses the traits of sparse queries, sparse attention and sparse prediction, and is able to efficiently extract and fuse cross-view features. Our insight is that box-feature twin-track proposals and cascade-style refinement process with only local RoI attention enable 3D object detection and cross-view fusion. We hope that this architecture can serve as a foundation for fully-sparse surround-view 3D object detection. In the future, the authors will investigate deeper in combining segmentation and temporal information to enhance the accuracy and robustness of SRCN3D.

References

- Bernardin, K.; and Stiefelhagen, R. 2008. Evaluating Multiple Object Tracking Performance: The CLEAR MOT Metrics. *J. Image Video Process.*, 2008.
- Caesar, H.; Bankiti, V.; Lang, A. H.; Vora, S.; Liong, V. E.; Xu, Q.; Krishnan, A.; Pan, Y.; Baldan, G.; and Beijbom, O. 2020. nuscenes: A multimodal dataset for autonomous driving. In *Proceedings of the IEEE/CVF conference on computer vision and pattern recognition*, 11621–11631.
- Carion, N.; Massa, F.; Synnaeve, G.; Usunier, N.; Kirillov, A.; and Zagoruyko, S. 2020. End-to-end object detection with transformers. In *European conference on computer vision*, 213–229. Springer.
- Chaabane, M.; Zhang, P.; Beveridge, J. R.; and O’Hara, S. 2021. Deft: Detection embeddings for tracking. *arXiv preprint arXiv:2102.02267*.
- Chen, H.; Wang, P.; Wang, F.; Tian, W.; Xiong, L.; and Li, H. 2022a. EPro-PnP: Generalized End-to-End Probabilistic Perspective-n-Points for Monocular Object Pose Estimation. In *Proceedings of the IEEE/CVF Conference on Computer Vision and Pattern Recognition*, 2781–2790.
- Chen, S.; ; Wang, X.; Cheng, T.; Zhang, Q.; Huang, C.; and Liu, W. 2022b. Polar Parametrization for Vision-based Surround-View 3D Detection. *arXiv:2206.10965*.
- Chiu, H.-K.; Li, J.; Ambruş, R.; and Bohg, J. 2021. Probabilistic 3D Multi-Modal, Multi-Object Tracking for Autonomous Driving. In *2021 IEEE International Conference on Robotics and Automation (ICRA)*, 14227–14233.
- Duan, K.; Bai, S.; Xie, L.; Qi, H.; Huang, Q.; and Tian, Q. 2019. Centernet: Keypoint triplets for object detection. In *Proceedings of the IEEE/CVF international conference on computer vision*, 6569–6578.
- García-Fernández, A.; Williams, J.; Granström, K.; and Svensson, L. 2017. Poisson multi-Bernoulli mixture filter: direct derivation and implementation. *IEEE Transactions on Aerospace and Electronic Systems*, PP.
- Gu, J.; Hu, C.; Zhang, T.; Chen, X.; Wang, Y.; Wang, Y.; and Zhao, H. 2022. ViP3D: End-to-end Visual Trajectory Prediction via 3D Agent Queries. *arXiv preprint arXiv:2208.01582*.
- He, K.; Zhang, X.; Ren, S.; and Sun, J. 2016. Deep residual learning for image recognition. In *Proceedings of the IEEE conference on computer vision and pattern recognition*, 770–778.
- Hu, H.-N.; Yang, Y.-H.; Fischer, T.; Darrell, T.; Yu, F.; and Sun, M. 2022. Monocular quasi-dense 3d object tracking. *IEEE Transactions on Pattern Analysis and Machine Intelligence*.
- Huang, J.; and Huang, G. 2022. Bevdet4d: Exploit temporal cues in multi-camera 3d object detection. *arXiv preprint arXiv:2203.17054*.
- Huang, J.; Huang, G.; Zhu, Z.; and Du, D. 2021. Bevdet: High-performance multi-camera 3d object detection in bird-eye-view. *arXiv preprint arXiv:2112.11790*.
- Lee, Y.; and Park, J. 2020. Centermask: Real-time anchor-free instance segmentation. In *Proceedings of the IEEE/CVF conference on computer vision and pattern recognition*, 13906–13915.
- Li, Z.; Wang, W.; Li, H.; Xie, E.; Sima, C.; Lu, T.; Yu, Q.; and Dai, J. 2022. BEVFormer: Learning Bird’s-Eye-View Representation from Multi-Camera Images via Spatiotemporal Transformers. *arXiv preprint arXiv:2203.17270*.
- Lin, T.-Y.; Dollár, P.; Girshick, R.; He, K.; Hariharan, B.; and Belongie, S. 2017a. Feature pyramid networks for object detection. In *Proceedings of the IEEE conference on computer vision and pattern recognition*, 2117–2125.
- Lin, T.-Y.; Goyal, P.; Girshick, R.; He, K.; and Dollár, P. 2017b. Focal loss for dense object detection. In *Proceedings of the IEEE international conference on computer vision*, 2980–2988.
- Liu, Y.; Wang, T.; Zhang, X.; and Sun, J. 2022a. Petr: Position embedding transformation for multi-view 3d object detection. *arXiv preprint arXiv:2203.05625*.
- Liu, Y.; Yan, J.; Jia, F.; Li, S.; Gao, Q.; Wang, T.; Zhang, X.; and Sun, J. 2022b. PETRv2: A Unified Framework for 3D Perception from Multi-Camera Images. *arXiv preprint arXiv:2206.01256*.
- MMDetection3D Contributors. 2020. MMDetection3D: OpenMMLab next-generation platform for general 3D object detection. <https://github.com/open-mmlab/mmdetection3d>.
- Park, D.; Ambrus, R.; Guizilini, V.; Li, J.; and Gaidon, A. 2021. Is pseudo-lidar needed for monocular 3d object detection? In *Proceedings of the IEEE/CVF International Conference on Computer Vision*, 3142–3152.
- Phillion, J.; and Fidler, S. 2020. Lift, Splat, Shoot: Encoding Images From Arbitrary Camera Rigs by Implicitly Unprojecting to 3D. In *Proceedings of the European Conference on Computer Vision*.
- Sun, P.; Zhang, R.; Jiang, Y.; Kong, T.; Xu, C.; Zhan, W.; Tomizuka, M.; Li, L.; Yuan, Z.; Wang, C.; et al. 2021. Sparse r-cnn: End-to-end object detection with learnable proposals. In *Proceedings of the IEEE/CVF conference on computer vision and pattern recognition*, 14454–14463.
- Wang, T.; Xinge, Z.; Pang, J.; and Lin, D. 2022. Probabilistic and geometric depth: Detecting objects in perspective. In *Conference on Robot Learning*, 1475–1485. PMLR.
- Wang, T.; Zhu, X.; Pang, J.; and Lin, D. 2021a. Fcos3d: Fully convolutional one-stage monocular 3d object detection. In *Proceedings of the IEEE/CVF International Conference on Computer Vision*, 913–922.
- Wang, Y.; Guizilini, V. C.; Zhang, T.; Wang, Y.; Zhao, H.; and Solomon, J. 2021b. DETR3D: 3D Object Detection from Multi-view Images via 3D-to-2D Queries. In *5th Annual Conference on Robot Learning*.
- Weng, X.; Wang, J.; Held, D.; and Kitani, K. 2020. Ab3dmot: A baseline for 3d multi-object tracking and new evaluation metrics. *arXiv preprint arXiv:2008.08063*.
- Xie, E.; Yu, Z.; Zhou, D.; Phillion, J.; Anandkumar, A.; Fidler, S.; Luo, P.; and Alvarez, J. M. 2022. M²BEV: Multi-Camera Joint 3D Detection and Segmentation with Unified Birds-Eye View Representation. *arXiv preprint arXiv:2204.05088*.

Zhang, R.; Qiu, H.; Wang, T.; Xu, X.; Guo, Z.; Qiao, Y.; Gao, P.; and Li, H. 2022a. Monodetr: Depth-aware transformer for monocular 3d object detection. *arXiv preprint arXiv:2203.13310*.

Zhang, T.; Chen, X.; Wang, Y.; Wang, Y.; and Zhao, H. 2022b. MUTR3D: A Multi-camera Tracking Framework via 3D-to-2D Queries. In *Proceedings of the IEEE/CVF Conference on Computer Vision and Pattern Recognition*, 4537–4546.

Zhou, X.; Koltun, V.; and Krähenbühl, P. 2020. Tracking objects as points. In *European Conference on Computer Vision*, 474–490. Springer.

Zhu, B.; Jiang, Z.; Zhou, X.; Li, Z.; and Yu, G. 2019. Class-balanced grouping and sampling for point cloud 3d object detection. *arXiv preprint arXiv:1908.09492*.

Zhu, X.; Su, W.; Lu, L.; Li, B.; Wang, X.; and Dai, J. 2020. Deformable detr: Deformable transformers for end-to-end object detection. *arXiv preprint arXiv:2010.04159*.